npj | clean water

www.nature.com/npjcleanwater

ARTICLE OPEN

Check for updates

Elimination of chloramphenicol through electro-fenton-like reaction: Reaction mechanism and electron transfer pathway

Meng Li[1,2✉], Ji-Liang Cheng[1], Jiayu Song[2], Zhao-Xin Zhang[3], Qiong Wu[2], Hai-Ming Zhao[1], Nai-Xian Feng[1], Wei Han[4,5], King Lun Yeung[2,4,5✉], Shaoqi Zhou[6✉] and Ce-Hui Mo[1✉]

An electro-Fenton-like reaction process relying on peroxymonosulfate activation can stably degrade chloramphenicol (CAP) within 16 min, where the kinetic rate constant can be as high as 0.089 min^{-1} and the energy consumption value can be as low as 25.1 kWh•m^$^{-3}$. Evidence indicated that the use of a Na_2SO_4 solution as the electrolyte can enhance CAP degradation due to rapid electron transfer properties. The generated electrons and active free radicals are responsible for CAP degradation, and the electrons can be transferred from the highest occupied molecular orbital of CAP to the lowest unoccupied molecular orbital of peroxymonosulfate via the PbO_2 electrode. Density functional theory calculations based on Fukui index analysis elucidated the key attack sites in CAP; moreover, reaction-free energy calculations shed light on potential CAP degradation pathways. Not only does this study afford an insight into the activation of peroxymonosulfate for organic pollutant degradation but also provides an innovative technology with potential applications in wastewater purification.

npj Clean Water (2023)6:39 ; https://doi.org/10.1038/s41545-023-00255-9

INTRODUCTION

The wide use of antibiotics for treating bacterial infections poses a substantial threat to human health and aquatic organisms due to the emergence of antibiotic resistance genes and antibiotic-resistant bacteria[1]. Chloramphenicol (CAP), a widely used broad-spectrum chlorinated nitroaromatic antibiotic, is often used in aquaculture, clinical practice, and poultry farming due to its low price and broad antibacterial properties[2]. CAP has been detected in concentrations ranging from ng L^{-1} to mg L^{-1} in groundwater, surface water, and soil[3]. The release of CAP even at trace concentrations (ng L^{-1}) is a potential environmental hazard[4]. Ingestion of excessive amounts of CAP is associated with aplastic anemia, kidney and liver damage, leukemia, and bone marrow toxicity[2,5]. Conventional wastewater treatment plants cannot effectively and completely remove CAP due to this compound's complex structure[6]. Therefore, developing efficient methods for CAP removal from aqueous media is a prime research goal.

Conventional technologies currently employed to remove antibiotics are based on biodegradation, coagulation, filtration, and adsorption[7,8]. Biodegradation methods are difficult to implement because of their relatively harsh operating conditions[9]. In coagulation processes, large amounts of sewage are released, potentially leading to secondary pollution[10]. Although membrane filtration affords the efficient removal of antibiotics, the associated high operating and maintenance costs limit its application[7]. Adsorption only transfers CAP from the liquid to the solid state, a process with substantial potential environmental risks[11]. Recently, advanced oxidation processes (AOPs) based on the persulfate ion and the generation of reactive oxygen species (ROS) have attracted considerable interest as convenient approaches for the treatment of various wastewater (such as oily wastewaters, landfill leachate, denitrification with Fenton-oxidized non-degradable large molecular organic pollutants, and removal of phosphorus)[12–14]. However, the preparation and use of various catalysts in AOPs increase the cost of contaminant removal.

Electrochemical AOPs are advantageous, given their operational simplicity and high stability as well as the low secondary pollution they cause; a range of organic pollutants have been efficiently degraded via these processes[15,16]. The electrochemical oxidation (EO) process effectively eliminated organic pollutants with the use of anode materials. Various electrodes, such as noble metals, carbon-based materials, boron-doped diamond, and two-/three-dimensional metal anodes (such as Ti_4O_7, IrO_2, and SnO_2), have been extensively studied and applied in the EO process for organic pollutant removal[17–20]. However, the prohibitive cost and the release of toxic metal ions associated with these electrodes have hindered their large-scale application for wastewater treatment. Recently, PbO_2 electrodes have been applied in electrocatalytic oxidation–based pollutant degradation as anodes owing to their high corrosion resistance, conductivity, oxygen evolution potential, catalytic activity, current transfer properties, and low cost[21,22]. Many researchers are working toward enhancing the electrochemical activity and stability of PbO_2 electrodes by introducing metal ions or oxides in them[23,24]. Although these modifications could greatly enhance the electrode's performance, they also require complex preparation methods that increase production costs. However, long-term use of PbO_2 electrodes poses a risk of releasing Pb ions into the environment, which can cause secondary pollution.

To address this issue, the present study implemented electrodeposition to simplify the electrode preparation process and reduce the leaching of metal ions while maintaining the electrode's high electrochemical activity and stability. By

[1]Guangdong Provincial Research Center for Environment Pollution Control and Remediation Materials, College of Life Science and Technology, Jinan University, Guangzhou 510632, PR China. [2]Department of Chemical and Biological Engineering, The Hong Kong University of Science and Technology, Clear Water Bay, Kowloon, Hong Kong, PR China. [3]Division of Emerging Interdisciplinary Areas, Hong Kong University of Science and Technology, Clear Water Bay, Kowloon, Hong Kong, PR China. [4]Division of Environment and Sustainability, The Hong Kong University of Science and Technology, Clear Water Bay, Kowloon, Hong Kong, PR China. [5]HKUST Shenzhen-Hong Kong Collaborative Innovation Research Institute, Futian, Shenzhen, Guangdong Province, China. [6]College of Resources and Environmental Engineering, Guizhou University, 2708 Huaxi Road, Guiyang 550025, PR China. ✉email: kemengli2020@gmail.com; kekyeung@ust.hk; zhousq@gzu.edu.cn; tchmo@jnu.edu.cn

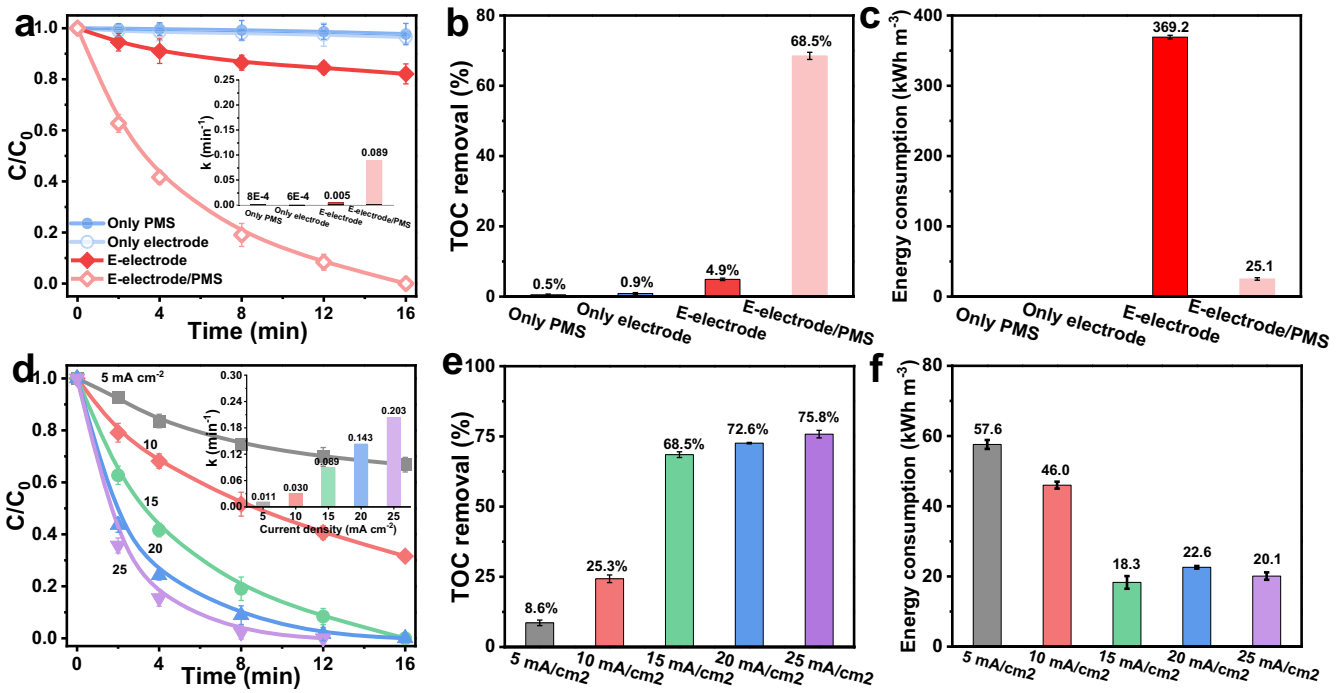

Fig. 1 Oxidation behavior of CAP. a Efficiency of chloramphenicol (CAP) degradation under different conditions: peroxymonosulfate alone (only PMS), an electrode with no electrochemical process (only electrode), an electrochemical process (E-electrode), and an electrochemical process in the presence of PMS (E-electrode/PMS). **b** Corresponding total organic carbon (TOC) removal rate and (**c**) energy consumption data. **d** Effects of different current densities on the efficiency of CAP degradation through electrochemical oxidation. **e** Corresponding TOC removal rates and (**f**) energy consumption data. Conditions: initial PMS concentration = 10 mM; initial CAP concentration = 5 mg L^{-1}; current density = 15 mA cm^{-2}; initial Na_2SO_4 concentration = 20 mM L^{-1}; temperature = 27 °C ± 2 °C.

increasing the current density and pulse frequency during the electrodeposition process, the average size of the electrode's particles could be regulated through morphological modification, causing the electrochemical activity of the electrode to increase via the generation of larger amounts of active centers and active free radicals[25]. An electro-Fenton-like reaction system relying on peroxymonosulfate (PMS) activation was manufactured for CAP degradation. Due to the high stability of this electrode and the use of low current density, no metal ions will be released from the electrode. In this study, the impact of the electrolyte (Na_2SO_4, $NaNO_3$, or $NaHCO_3$) on the efficiency of CAP degradation combined with density functional theory (DFT) calculations were explored to address the following issues: (i) why do some electrolytes afford increases in the efficiency of electrochemical systems in the degradation organic pollutants? (ii) How do electrolytes assist the transfer of the electrons involved in the electrochemical reaction? (iii) Where are the key reaction and binding sites of the electrode and electrolyte located that are responsible for the EO process? Moreover, the degradation of CAP may involve dichlorination, dehydration, substitution, hydrolysis, and oxidation[26,27]. The researchers employed mass spectroscopy and DFT calculations to investigate the reaction sites, radical release pathways, and electron transfer and excitation properties of CAP to determine the CAP degradation pathway for various dissociation sites. Additionally, the contributions to the observed reactivity of different ROS were determined by conducting scavenger quenching and electron paramagnetic resonance (EPR) spectroscopy experiments. The ecotoxicities of CAP and its degradation intermediates were also predicted for risk assessment. Moreover, the stability and application potential of the electro-Fenton-like reaction process for CAP degradation was demonstrated based on the results of recycling operations and the effects different water matrices had on the efficiency of CAP-pollution remediation. The overall aim of this study is to gain a deeper understanding of the mechanism of CAP degradation driven by free radical reactivity via the electro-Fenton-like reaction system.

RESULTS AND DISCUSSION

CAP oxidation behavior

Figure 1 shows the data reflecting the behavior of CAP oxidation under different conditions; the values of the relevant kinetic rate constants were obtained by fitting the experimental CAP oxidation data with a pseudo-first-order equation. CAP can be degraded under EO conditions without PMS; however, under such conditions, only 17.9% of CAP was removed within 16 min. After adding PMS to the electrolyte solution to a final 10 mM concentration, CAP underwent complete degradation within 16 min and a high kinetic rate constant of 0.089 min^{-1} was obtained for the process, which was significantly larger than the corresponding parameter for the purely electrochemical process (0.005 min^{-1}). PMS by itself did not degrade CAP, while the anode alone exhibited only a very slight CAP adsorption capacity, indicating that PMS played a critical role in CAP degradation. Hence, the addition of PMS to the electrolyte can result in the generation of active radicals that cause CAP to degrade under electrochemical conditions; the relevant reaction process is similar to a Fenton-like reaction; therefore, we denoted the electrochemical process occurring in the presence of PMS as an electro-Fenton-like reaction. In the absence of PMS, CAP can be directly oxidized on the surface of the PbO_2 electrode through direct electron transfer. However, in the presence of PMS, the PbO_2 electrode activates the PMS, transforming it into a special transition state structure (HSO_5^{-}*) that exhibits stronger oxidizing power toward organic compounds (as shown in Eq. (1)). Furthermore, PbO_2(HSO_5^{-}*) can also decompose to generate •OH and $SO_4^{\bullet-}$ radicals (Eq. (2)). Additionally, the generated •OH

radicals can react with PMS to form $SO_4^{\bullet -}$ radicals (Eq. (3)). Notably, PMS can also capture an electron on the electrode, generating •OH and $SO_4^{\bullet -}$ radicals (Eq. (4)). The transition state structure and generated radicals greatly enhanced the degradation efficiency of CAP.

$$PbO_2 + HSO_5^- \rightarrow PbO_2\text{-}HSO_5^- \rightarrow PbO_2(HSO_5^{-*}). \quad (1)$$

$$PbO_2(HSO_5^{-*}) \rightarrow \cdot OH + SO_4^{\cdot -}. \quad (2)$$

$$HSO_5^- + \cdot OH \rightarrow SO_4^{\cdot -} + H_2O + 0.5\,O_2. \quad (3)$$

$$HSO_5^- + e^- \rightarrow SO_4^{\cdot -} + OH^- \text{or } \cdot OH + SO_4^{2-}. \quad (4)$$

To explore the electrode performance for CAP degradation, TOC removal efficiencies were determined during CAP degradation. The electro-Fenton-like process afforded a TOC removal efficiency of 68.6% (Fig. 1b), which is substantially higher than that achieved through the electrochemical process without PMS (4.9%). During the electro-Fenton-like reaction, the electric energy per order (EE/O) was considered a key indicator of energy consumption, and its value was calculated using Eq. (5).

$$EE/O = Ult \times 1000/(60V \times \lg(C_0/C_t)) \quad (5)$$

where U and I are the output voltage (V) and current (A), respectively, t is the reaction time (h), V is the reactor volume (L), and C_0 and C_t are the CAP concentrations at time 0 and t, respectively. As can be evidenced from Fig. 1c, the EE/O associated with the electro-Fenton-like process (25.1 kWh•m^{-3}) was much lower than the EE/O associated with the electrochemical process conducted without PMS (369.2 kWh•m^{-3}), which suggests that PMS use can effectively reduce energy consumption. Overall, the low energy consumption, high kinetic rate constant, and high TOC removal efficiency indicate that the electro-Fenton-like process was more energy-efficient than the traditional electrochemical process.

Current density is considered an important factor in the degradation of organic pollutants as it determines the ROS generation rate[28]. Only 33.2% of CAP was removed under electro-Fenton-like reaction conditions when the initial current density was 10 mA cm^{-2} (Fig. 1d). CAP removal efficiency gradually increased as the current density grew from 5 to 25 mA cm^{-2}. Nearly 100% of CAP was removed at 15, 20, and 25 mA cm^{-2} current densities during 12–16 min electrolysis processes. All the CAP removal processes followed pseudo-first-order kinetics; moreover, the kinetic rate constant was determined to increase from 0.011 to 0.203 min^{-1} as the current density increased from 5 to 25 mA cm^{-2}. The data reported in Fig. 1e indicate that the TOC removal efficiency increasing with the current density. Notably, although the TOC removal efficiency increased to 75.8% at 25 mA cm^{-2} from 68.5% at 15 mA cm^{-2} and 72.6% at 20 mA cm^{-2}, the removal efficiency became less pronounced in comparison with that from 10 to 15 mA cm^{-2}. The EE/O was minimal at 15 mA cm^{-2} (Fig. 1f); the parameter decreased to 18.3 kWh•m^$^{-3}$ as the current density increased from 5 to 15 mA cm^{-2}. In addition, the fact that at 15 mA cm^{-2} the EE/O value was much lower than at 20 mA cm^{-2} (22.6 kWh•m^$^{-3}$) and 25 mA cm^{-2} (20.1 kWh•m^$^{-3}$) suggests that performing the process at 15 mA cm^{-2} current density could efficiently decrease energy consumption. Consequently, imposing an initial current density of 15 mA cm^{-2} was beneficial to CAP degradation via an electro-Fenton-like reaction process.

As can be evinced from Supplementary Fig. 1, the CAP degradation rate was 17.9%, 70.5%, 100%, and 96.1% after 16 min of electrolysis, when the initial PMS concentration was 0, 5, 10, and 20 mM, respectively. The kinetic rate constant measured over 16 min of electrolysis increased from 0.005 to 0.089 min^{-1} as the initial PMS concentration increased from 0 to 10 mM. The highest kinetic rate constant was measured at a 10 mM initial PMS concentration, suggesting that at this concentration CAP degradation in the electro-Fenton-like process could be effectively boosted. The CAP degradation rate at 10 mM PMS initial concentration (0.089 min^{-1}) was ~17.8 and 2.8 times higher than at 0 (0.005 min^{-1}) and 5 mM (0.032 min^{-1}) initial PMS concentrations, respectively. At low initial PMS concentration, PMS cannot be effectively activated to generate active species for CAP degradation thereby exhibiting low removal efficiency and kinetic rate constant. However, due to quenching between •OH/$SO_4^{\bullet -}$ and PMS, the kinetic rate constant did not increase further as the initial PMS concentration increased from 10 to 20 mM[29]. These findings indicate that the electro-Fenton-like process conducted in the presence of an initial PMS concentration of 10 mM can afford the effective degradation of CAP.

Effect of the electrolyte on CAP oxidation

The electrolyte determines the electron transfer efficiency during the electrochemical process and influences PMS activation and ROS generation. To explore the effect of different electrolytes, CAP degradation was also conducted in $NaHCO_3$ and $NaNO_3$ solutions with the same concentration as 1000 mg L^{-1} Na_2SO_4 (3.4 mS cm^{-1}). After conducting 16 min electrolysis using a PbO_2 electrode at 15 mA cm^{-2} current density, the CAP removal rate was 92.3% in $NaHCO_3$ solution and 74.9% in $NaNO_3$ solution (Fig. 2a); under the same conditions, the CAP removal rate was nearly 100% in the Na_2SO_4 solution. Moreover, the kinetic rate constant for CAP oxidation in the Na_2SO_4 solution was 1.33 and 2.28 times higher than in $NaHCO_3$ and $NaNO_3$ solutions, respectively. Similarly, the TOC removal efficiency (Fig. 2b) was significantly higher in the Na_2SO_4 solution (68.5%) than in $NaHCO_3$ (56.9%) and $NaNO_3$ (49.3%) solutions. Moreover, we determined the electric consumption levels of different electrolytes. The EE/O of the CAP degradation process conducted in the Na_2SO_4 solution (25.1 kWh•m^$^{-3}$) was much lower than the EE/O of the process conducted in the $NaHCO_3$ (36.3 kWh•m^$^{-3}$) and $NaNO_3$ (53.1 kWh•m^$^{-3}$) solutions (Fig. 2c), which further confirmed the effectiveness of the Na_2SO_4 solution as the electrolyte for the process of CAP degradation under electro-Fenton-like reaction conditions.

To determine the reason for the effective performance of CAP degradation in Na_2SO_4 solution than in the other electrolytes, the electrochemical properties of PbO_2 were investigated using an electrochemical workstation with different electrolytes. Although the obtained CV curves exhibited similar morphologies, the curve recorded in the Na_2SO_4 solution had a larger area than those recorded in the $NaHCO_3$ and $NaNO_3$ solutions (Fig. 2d). These results indicate that, in the Na_2SO_4 solution, the electrode possessed a larger capacitance than in the other solutions; the larger the capacitance, the more facile the electron transfer and the electrochemical reaction. The LSV curves of PbO_2 reported in Supplementary Fig. 2 indicate that the current density of the electrode in the Na_2SO_4 solution was much higher than the corresponding parameter measured in the $NaHCO_3$ and $NaNO_3$ solutions when the potential was more positive than 0.8 V, which may be ascribed to rapid electron transfer. We also conducted EIS experiments on the PbO_2 electrode in the mentioned electrolytes. Generally, the ohmic resistance of the electrode would be determined by the characteristics of the electrode. Consequently, similar electrodes used in different electrolytes exhibited similar ohmic resistance (Fig. 2e). However, the electrode's charge transfer resistance was significantly larger in the $NaHCO_3$ and $NaNO_3$ solutions than in the Na_2SO_4 solution. A previous report confirmed that a low value for the charge transfer resistance was beneficial to the efficiency of the electron transfer[30]; therefore, a rapid electron transfer and electrochemical reaction occurred in the $NaSO_4$ solution. In the Na_2SO_4 solution, the electrode exhibited a smaller Tafel slope and a larger exchange current

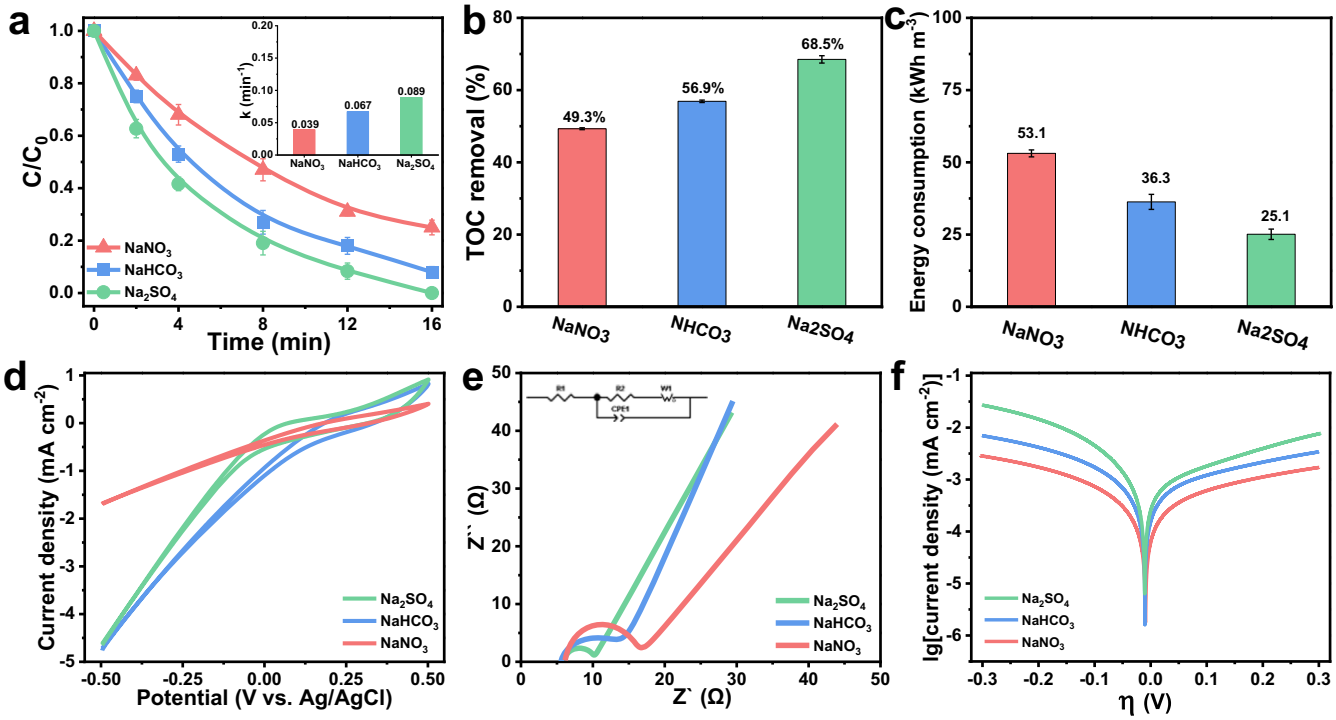

Fig. 2 The effect pf electrolyte properties on CAP degradation. a Efficiency of CAP degradation on a PbO_2 electrode using different electrolytes (1000 mg/L), and the corresponding (**b**) TOC removal rates and (**c**) energy consumption values. **d** Cyclic voltammograms, (**e**) electrochemical impedance spectroscopy contours, and (**f**) Tafel curves obtained for the PbO_2 electrode using different electrolytes.

density than in the $NaHCO_3$ and $NaNO_3$ solutions (Fig. 2f), indicating that the electron transfer was faster and the electrochemical activity was higher in the Na_2SO_4 solution than in the other electrolytes. The results of the investigations discussed above may demonstrate the high electron transfer efficiency and electrochemical activity of the PbO_2 electrode in the Na_2SO_4 solution for CAN degradation under electro-Fenton-like reaction conditions.

Based on the abovementioned results, we modeled the interactions between the electrode and the electrolytes (Na_2SO_4, $NaHCO_3$, and $NaNO_3$). The data in Fig. 3 indicate that these electrolytes (SO_4^{2-}, HCO_3^-, and NO_3^-) were adsorbed on the electrode surface, and the O centers in the electrolytes can be strongly adsorbed on the electrode surface through the formation of Pb–O bonds. The obtained electron density data also suggest that the O atoms in the electrolyte anions participate in the electron transfer process through the formed Pb–O bonds. In the case of Na_2SO_4, the length of the Pb–O bond was estimated to be 2.307 Å, which is a much smaller value than those computed for $NaHCO_3$ (2.347 Å) and $NaNO_3$ (2.372 Å). Results from a previous report indicated that long adsorption bonds are unstable; hence, the adsorbed species are easily separated from the electrode surface[31]. Thus, the chemical bonds formed between the electrode and the HCO_3^- or NO_3^- anions were much weaker than that between the electrode and SO_4^{2-}. Duan et al. reported that the formation of short chemical bonds during adsorption accelerated the electron transfer and enhanced the efficiency of the electrochemical reaction[32]. Consequently, the electrochemical reaction was much faster in the Na_2SO_4 solution than in the $NaHCO_3$ or $NaNO_3$ solution. The molecular orbitals after adsorption were also calculated. The highest occupied molecular orbital (HOMO) was associated with the outermost larger energy orbital employing as the electron donor, while the lowest unoccupied molecular orbital (LUMO) was related to the electron acceptor[33]. Ayyappan et al. proved that the HOMO–LUMO energy gap and the relevant molecular orbital energies could reflect the stability of chemical bonds[34]. As evinced from Fig. 3, the HOMO–LUMO energy gap was the largest for the Na_2SO_4–electrode interaction (0.0763 eV), intermediate for the $NaHCO_3$–electrode interaction (0.0759 eV), and smallest for the $NaNO_3$–electrode interaction (0.0717 eV). The strongest chemical bond could thus be formed between the electrode and $NaSO_4$ solution, thereby exhibiting stable electron transfer and electrochemical reaction. Accordingly, the Na_2SO_4 solution played a critical role in binding electrodes for effective electron migration during the electro-Fenton-like process.

Identification and contribution of ROS

To determine the contribution of ROS to CAP degradation during the electro-Fenton-like reaction, CAP electrolysis was conducted on a PbO_2 electrode in the presence of different radical scavengers. MeOH, TBA, BQ, and NaN_3 were chosen to quench $SO_4^{\bullet-}$, •OH, $O_2^{\bullet-}$, and $^1O_2$, respectively[35,36]. The inhibitory effect of MeOH was obvious (Fig. 4a): CAP removal efficiency decreased from 100% to 92.4% following the addition of MeOH to a final 10-mM concentration; additionally, the corresponding kinetic rate constant decreased from 0.089 to 0.068 min^{-1}. The rate constant declined further to 0.024 and 0.006 min^{-1} as the final MeOH concentration increased to 25 and 50 mM, respectively. In the presence of 25 mM TBA (Fig. 4b), CAP removal efficiency decreased to 95.2%, and this parameter decreased further to 74.7% as TBA concentration increased to 50 mM. The kinetic rate decreased from 0.089 to 0.037 min^{-1} as TBA concentration increased from 0 to 50 mM. However, no significant inhibition of CAP removal was observed following the addition of BQ or NaN_3 (Fig. 4c, d); the corresponding kinetic rate constants also remained stable as the mentioned scavengers' concentrations increased from 10 to 50 mM. These results indicated that $^1O_2$ and $O_2^{\bullet-}$ were not generated or involved in CAP degradation via the electro-Fenton-like reaction. However, the decline in CAP degradation performance induced by MeOH and TBA suggested that •OH and

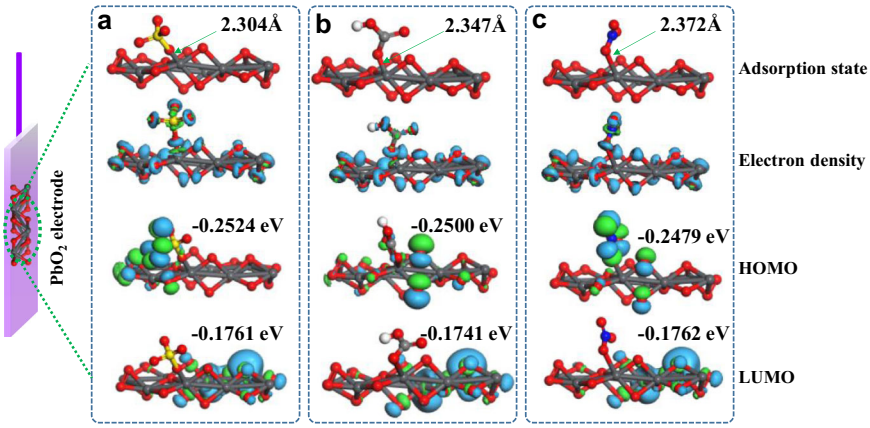

Fig. 3 Electrolyte adsorption model. Results of the density functional theory calculations performed to estimate the magnitude of the interaction between the PbO_2 electrode and different electrolytes: **a** Na_2SO_4, (**b**) $NaHCO_3$, and (**c**) $NaNO_3$ solutions.

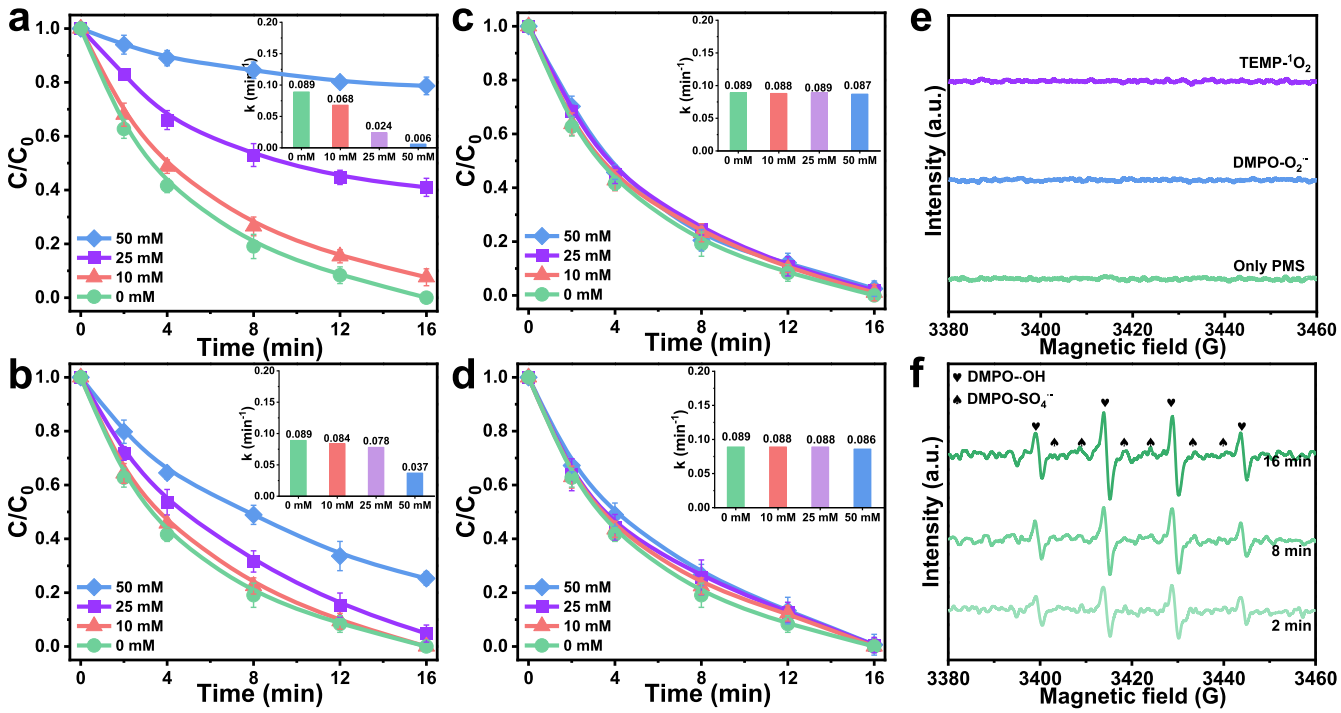

Fig. 4 Identification of active species. Effects of various concentrations of (**a**) methanol, (**b**) *tert*-butanol, (**c**) 1,4-benzoquinone, and (**d**) NaN_3 on the efficiency of chloramphenicol oxidation. Electron paramagnetic resonance spectra of (**e**) $^1O_2$ and $O_2^{\cdot-}$ and (**f**) ·OH and $SO_4^{\cdot-}$. DMPO: 5,5-dimethyl-1-pyrroline-N-oxide; TEMP: 2,2,6,6-tetramethyl-4-piperidinyloxyl.

$SO_4^{\cdot-}$ were the key active species in CAP degradation. Based on the discussed results, we can infer that the relative contributions of •OH, $SO_4^{\cdot-}$, and electrode-provided electrons to the electro-Fenton-like reaction–driven degradation of CAP were 58.5%, 34.8%, and 6.7%, respectively.

EPR spectroscopy experiments were conducted in the presence of spin-trapping agents—TEMP and DMPO—to investigate TOS generation during the electro-Fenton-like process using the PbO_2 electrode. No peaks attributable to the TEMP–$^1O_2$ or DMPO–$O_2^{\cdot-}$ spin adducts were observed (Fig. 4e), suggesting that $^1O_2$ and $O_2^{\cdot-}$ were not generated during the electro-Fenton-like reaction. No obvious signal was detected in the presence of only PMS, suggesting that PMS by itself was unable to generate ROS. These results agreed with the results of the radical scavenging tests. A characteristic four-line peak with a 1:2:2:1 intensity ratio was observed (Fig. 4f), which indicated that a DMPO–•OH spin adduct had been produced[37], confirming the generation of •OH radicals during the electro-Fenton-like reaction. The six-line characteristic signals (1:1:1:1:1:1) due to the DMPO–$SO_4^{\cdot-}$ spin adduct was also detected[38], indicating the formation of $SO_4^{\cdot-}$ during the process leading to CAP degradation. The intensities of the signals due to the DMPO–•OH and DMPO–$SO_4^{\cdot-}$ spin adducts increased as the reaction time increased from 2 to 16 min, suggesting the gradual generation of •OH and $SO_4^{\cdot-}$ species. The intensity of the peak due to DMPO–•OH was much higher than that due to DMPO–$SO_4^{\cdot-}$, which may indicate that •OH radicals were produced in much larger numbers than $SO_4^{\cdot-}$ radicals. The results of the EPR spectroscopy analysis are consistent with the evidence obtained from the scavenging

tests, leading to the conclusion that the electro-Fenton-like reaction performed using the PbO_2 electrode could effectively activate PMS to generate •OH and $SO_4^{\bullet-}$ radicals for CAP degradation.

To trace the origin of the oxygen atoms in these radicals, different gases (air, N_2, O_2, and Ar) were bubbled into the electrolyte to explore the effect that they had on CAP degradation efficiency. As can be evinced from Supplementary Fig. 3, neither the kinetic rate constant of CAP degradation nor the TOC removal efficiency substantially differed between experiments. This observation indicated that the oxygen atoms in •OH and $SO_4^{\bullet-}$ originated from the electrochemical reaction and not from electrolyte-dissolved molecular oxygen. Consequently, the •OH and $SO_4^{\bullet-}$ radicals generated in the electro-Fenton-like reaction were responsible for CAP degradation.

Reaction mechanism

The reaction mechanism and the possible pathway of radical generation were investigated while performing DFT calculations. The computational data reported in Fig. 5a suggest that PMS is first adsorbed on the electrode surface so that the PMS–PbO_2 structure is produced via the formation of the O–Pb bond characterized by a free energy of −1.79 eV; notably, a value this low for the free energy indicates that the described adsorption process is thermodynamically feasible at room temperature. Subsequently, the PMS–PbO_2 structure loses a OH– group to form a SO_4–PbO_2 structure because of the attacking effect of the electron along with a free energy of 2.56 eV. Under the electrochemical effect, the SO_4–PbO_2 structure may then capture a water molecule to generate •OH and form the HSO_4–PbO_2 structure, which is characterized by a free energy of 5.21 eV. Ultimately, $SO_4^{\bullet-}$ is generated due to the break-up of the unstable HSO_4–PbO_2 structure (ΔG = 3.12 eV). The $SO_4^{\bullet-}$ radicals then attack CAP, causing the compound's decomposition and degradation. These reactions and feasible free energies confirmed the generated pathway of the radicals. No Pb ions were detected in the electrolyte through inductively coupled plasma–optical emission spectroscopy (ICP–OES), suggesting that the PbO_2 electrode was highly stable during the electro-Fenton-like reaction process.

PMS present in the electrolyte is crucial for generating ROS to degrade organic pollutants. In this study, PMS was absorbed onto the surface of the PbO_2 electrode through a chemical bond formation. The S atom in PMS was surrounded by O atoms, while Pb and O elements covered the electrode surface. The chemical bond formed between the electrode and PMS in the electrolyte was either a Pb–O bond or an O–O bond. We further calculated the adsorbed energy of PMS on the electrode surface through the Pb–O or O–O bond connection. Our calculations revealed that the O atom in the PMS structure absorbed the O atom in the PbO_2 structure, forming the O–O bond, as shown in Supplementary Fig. 4. The formation of the Pb–O bond occurred due to the O atom in the PMS structure adsorbed onto the Pb atom in the PbO_2 structure. Importantly, the Pb–O bond had a shorter bond length (1.516 Å) than that of the O–O bond (1.699 Å), indicating a faster electron transfer between PMS and the electrode via the Pb–O bond. Moreover, the Pb–O bond exhibited more negative adsorption energy (−1.786 eV) than the O–O bond (−1.295 eV), indicating that PMS can be rapidly absorbed and participate in an electrochemical reaction on the surface of the PbO_2 electrode via the Pb–O bond. Consequently, the Pb–O bond played a crucial role in the electrochemical reaction for CAP degradation.

The features of the electron transfer between CAP and radicals were determined based on the HOMO–LUMO profiles and relevant energy gaps. Figure 5b illustrates the optimized geometrical configurations of PMS, PbO_2, CAP, $SO_4^{\bullet-}$, and •OH as well as the potential electron transfer pathway. The energy of

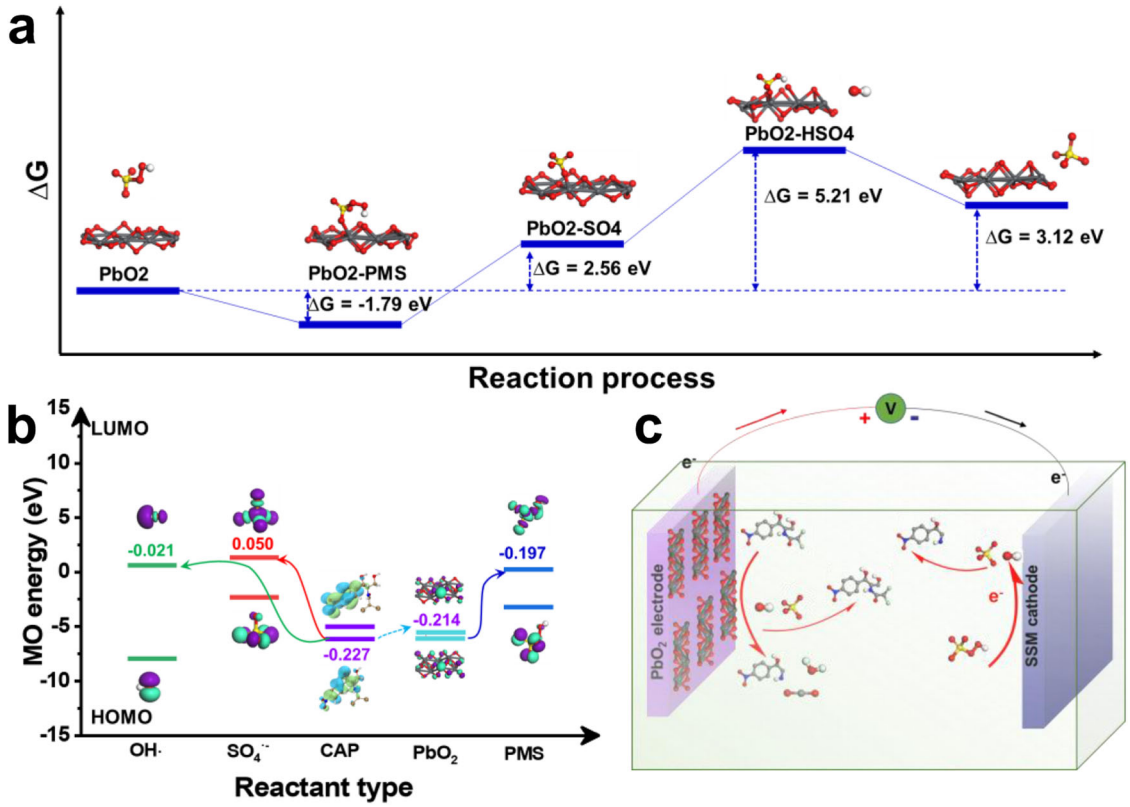

Fig. 5 Reaction mechanism. a Computed free energies profiles for the species assumed to be involved in the generation of $SO_4^{\bullet-}$ radicals. **b** Electron transfer pathways for CAP degradation. **c** Possible mechanism of CAP degradation under electrochemical conditions. HOMO Highest occupied molecular orbital, LUMO Lowest unoccupied molecular orbital, MO Molecular orbital.

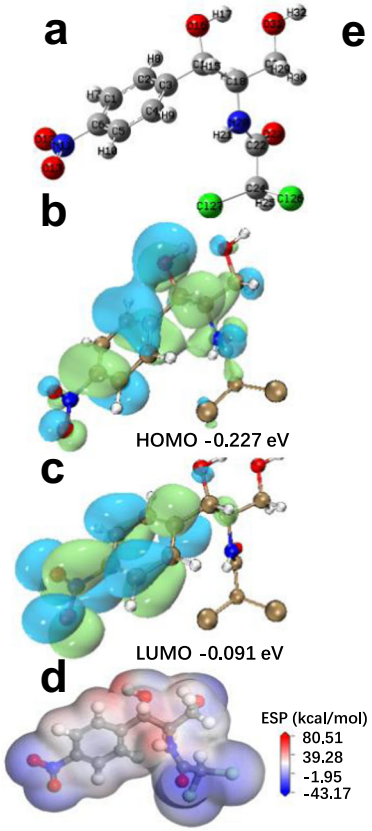

e

Atom	q(N)	q(N-1)	q(N+1)	f^+	f^-	f^0
1C	-0.14899	-0.13198	-0.17809	0.029096	0.017013	0.023055
2C	-0.17377	-0.14306	-0.18869	0.014929	0.030708	0.022819
3C	0.180662	0.187123	0.155237	0.025425	0.006461	0.015943
4C	-0.21715	-0.21344	-0.223	0.005848	0.003717	0.004783
5C	-0.14584	-0.11267	-0.18029	0.034446	0.033175	0.033811
6C	0.276412	0.323766	0.216696	0.059716	0.047354	0.053535
7H	0.18681	0.236355	0.131509	0.055301	0.049545	0.052423
8H	0.168861	0.216518	0.10809	0.060771	0.047657	0.054214
9H	0.143049	0.187669	0.080628	0.062421	0.04462	0.053521
10H	0.185937	0.239839	0.130143	0.055794	0.053902	0.054848
11N	0.340855	0.396368	0.291607	0.049248	0.055513	0.052381
12O	-0.39231	-0.34383	-0.53333	0.14102	0.048486	0.094753
13O	-0.3947	-0.34337	-0.5344	0.1397	0.05133	0.095515
14C	0.047596	0.016316	0.045483	0.002113	-0.03128	-0.01458
15H	0.119876	0.189095	0.085009	0.034867	0.069219	0.052043
16O	-0.65045	-0.55248	-0.65792	0.007468	0.097966	0.052717
17H	0.43157	0.464825	0.408866	0.022704	0.033255	0.02798
18C	0.009614	-0.01059	0.020616	-0.011	-0.0202	-0.0156
19H	0.18813	0.221778	0.173173	0.014957	0.033648	0.024303
20N	-0.62404	-0.58377	-0.69132	0.067285	0.040271	0.053778
21H	0.351457	0.370328	0.349543	0.001914	0.018871	0.010393
22C	0.63496	0.645932	0.622961	0.011999	0.010972	0.011486
23O	-0.48117	-0.39003	-0.52535	0.044177	0.091142	0.06766
24C	-0.41078	-0.42558	-0.41653	0.005751	-0.0148	-0.00452
25H	0.267287	0.299752	0.238228	0.029059	0.032465	0.030762
26Cl	-0.00025	0.074602	-0.07658	0.076328	0.074853	0.075591
27Cl	-0.00396	0.051761	-0.01652	0.012569	0.055716	0.034143
28C	-0.03875	-0.03715	-0.04262	0.003872	0.001601	0.002737
29H	0.134447	0.16995	0.116853	0.017594	0.035503	0.026549
30H	0.177368	0.210085	0.157618	0.01975	0.032717	0.026234
31O	-0.63759	-0.62898	-0.63718	-0.0004	0.008608	0.004102
32H	0.414852	0.444845	0.39557	0.019282	0.029993	0.024638

Fig. 6 Molecular properties of CAP. a Optimized molecular structure of CAP. **b** Highest occupied molecular orbital (HOMO). **c** Lowest unoccupied molecular orbital. **d** Electrostatic potential map of CAP. **e** Natural population analysis charge distribution and condensed Fukui index distribution of CAP.

the LUMO of PbO_2 (−5.214 eV) was much larger than that of the HOMO of CAP (−6.227 eV), which implies that electrons can be transferred from CAP to the PbO_2 electrode. The energy of the LUMO of PMS is also larger than that of the HOMO of the PbO_2 electrode (Fig. 5b), suggesting that the electrons can be further transferred from the PbO_2 electrode to PMS. Accordingly, during the electro-Fenton-like reaction, electrons could be transferred from low-energy HOMOs to high-energy LUMOs; hence, electrons can be transferred from CAP to PMS via the PbO_2 electrode. Furthermore, the PMS may capture the transferred electrons to generate $SO_4^{\bullet-}$ and •OH radicals. Electrons can be further transferred from low-energy orbitals of CAP to high-energy orbitals of the radicals. A CAP molecule that has lost some electrons can easily be attacked by $SO_4^{\bullet-}$ and •OH, bringing about CAP decomposition.

Based on the obtained experimental results and DFT calculations, we proposed a possible reaction mechanism for CAP degradation under electro-Fenton-like reaction conditions (Fig. 5c). PMS is first adsorbed on the surface of the PbO_2 electrode; following the electron transfer and electrochemical reaction, PMS then undergoes decomposition to produce $SO_4^{\bullet-}$ and •OH radicals. These species attack the key sites of CAP to trigger its decomposition and the formation of smaller molecular species, including CO_2 and H_2O. Therefore, CAP can be effectively removed from the solution and mineralized via the electro-Fenton-like reaction process.

CAP degradation pathway

To investigate the degradation pathway of CAP under electro-Fenton-like reaction conditions, Fukui indices were determined based on the results of DFT calculations, and GC–MS experiments were conducted to gather information on the degradation products of CAP. The optimized molecular structure of CAP (Fig. 6a) and the corresponding Fukui indices are calculated. The HOMO (Fig. 6b) and LUMO (Fig. 6c) were calculated to obtain the probability electron density distribution and charge values of CAP. Published studies have proven that the HOMO and LUMO correspond to electron-rich and electron-poor regions, respectively; hence, the HOMO can easily lose electrons as a result of an electrophilic attack, while the LUMO is prone to gaining electrons following a nucleophilic attack[39,40]. The Fukui indices of different atoms in CAP are reported in Fig. 6e; in this figure, f^-, f^+, and f^0 represent electrophilic attack, nucleophilic attack, and the degree of free radical attack, respectively[41,42]. 6C ($f^0 = 0.054$), 11 N ($f^0 = 0.052$), and 20 N ($f^0 = 0.054$) in the main carbon-chains are prone to being attacked by electrophilic radicals. In particular, ROS adsorbed in correspondence of 20 N brings about the cleavage of the 20N–C22 bond (pathway I: CAP → P1 → P3 → P5; see Fig. 7a), while adsorption in correspondence of 11 N results in the cleavage of the 11N–6C bond (pathway II: CAP → p2 → p4 → p6; see Fig. 7a). The characteristics of the HOMO (Fig. 6b), LUMO (Fig. 6c), and electrostatic potential map (Fig. 6d) of CAP also suggest that 11 N and 20 N are vulnerable to electrophilic attack, which would lead to the cleavage of chemical bonds.

Figure 7 reports the possible CAP degradation pathway, and information on the corresponding products is provided in Supplementary Table 1. In pathway I, 20 N is directly attacked by $•OH/SO_4^{\bullet-}$, leading to the cleavage of the 20N–C22 bond and the formation of intermediate P1 ($m/z = 212$). Notably, DFT calculations afforded a value for the Gibbs free energy for the generation of P1 of −0.85 eV (Fig. 7b), which suggests that P1 generation is thermodynamically feasible. Subsequently, the amino group on P1

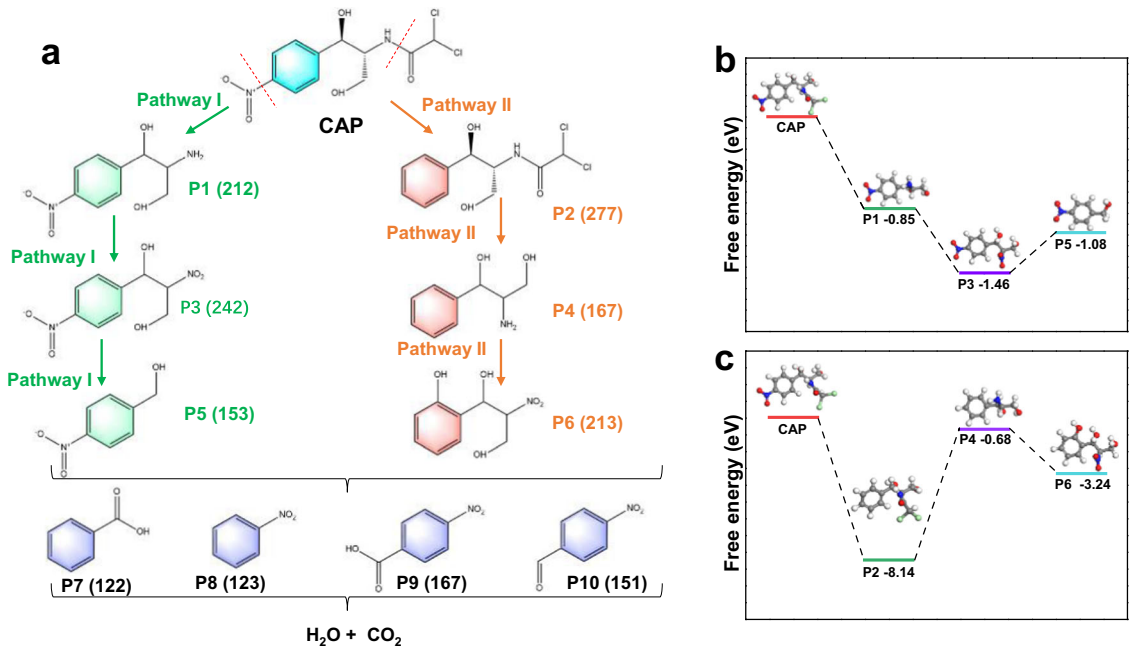

Fig. 7 Degradation behaviors of CAP. a Possible pathways for CAP degradation. Calculated free energies of CAP and the degradation intermediates produced in pathways (**b**) I and (**c**) II.

is oxidized by $\cdot OH/SO_4^{\cdot -}$, leading to the formation of P3 (m/z = 242), which is characterized by a free energy of −1.46 eV. Next, P3 is degraded by $\cdot OH/SO_4^{\cdot -}$. With the cleavage of the C14–C18 bond, compound P5 (m/z = 153) is generated along with low free energy (ΔG = −1.08 eV). In pathway II, attack by $\cdot OH/SO_4^{\cdot -}$ causes the 11N–6 C bond in the benzene ring of CAP to be cleaved so that product P2 (m/z = 277) is formed. The low free energy value for this process (ΔG = −8.14 eV; Fig. 7c) confirms the thermodynamic viability of the reaction route from CAP to P2. Compound P2 is then transformed to P4 (m/z = 167), in a similar way as pathway I, via the cleavage of the C–N bond (ΔG = −0.68 eV). Through oxidation of the amino group and a hydroxylation reaction, P4 is transformed to P6 (m/z = 213; ΔG = −3.24 eV). The reactions expected to occur in pathways I and II are thermodynamically spontaneous at room temperature as the relevant ΔG values are all negative; thus, the formed P5 and P6 products are oxidized to produce low-molecular-weight aromatic compounds, such as P7 (m/z = 122), P8 (m/z = 123), P9 (m/z = 167), and P10 (m/z = 151). Finally, these aromatic compounds undergo deep oxidization and are attacked by $\cdot OH/SO_4^{\cdot -}$, resulting in ring-opening reactions that produce short-chain organic acids, which are further decomposed and mineralized into inorganic molecules (e.g., CO_2 and H_2O).

The toxicities of CAP and its degradation intermediates produced during the electro-Fenton-like process were assessed by the T.E.S.T. software; the developmental factor, fathead minnow LC_{50}, and *Tetrahymena pyriformis* 50% inhibition growth concentration (IGC_{50}) values were obtained using the QSAR method[43]. As indicated by Supplementary Fig. 5a, CAP is considered a "developmental toxicant," while the herein-described oxidation process yielded degradation products of inferior toxicity to CAP; products P5, P7, P8, P9, and P10 are even defined as "developmental non-toxicant." The LC_{50} of fathead minnow for CAP was 1.61 mg L^{-1} (Supplementary Fig. 5b), which indicates that CAP can be considered "Toxic." As to the CAP degradation products, their acute toxicities were inferior to those of CAP, owing to their lower molecular weight; nevertheless, some of these products were still categorized as harmful, based on their LC_{50} values. The value of the 48 h *T. pyriformis* IGC_{50} of CAP was 32.8 mg L^{-1} (Supplementary Fig. 5c), which is significantly lower than those of CAP degradation products; in fact, all these products, except for P5 and P10, were "Not harmful," implying that the growth inhibition resulting from CAP exposure was much more significant than that caused by exposure to CAP degradation intermediates. Considering the high TOC removal efficiency (68.5%), we believed that not only did the electro-Fenton-like process reduce the toxicity of CAP but also mineralized these intermediate products into CO_2 and H_2O.

Stability and applied potential

To probe the adaptability of the PbO_2 electrode, different water matrices (distilled water, groundwater, seawater, and Pearl river water) were used as natural backgrounds to study the degradation performance of CAP under electro-Fenton-like reaction conditions. CAP could be effectively removed from different water matrices even in the presence of some background ions (Fig. 8a). Notably, the kinetic rate constant of CAP degradation in Pearl river water was slightly lower than in distilled water, groundwater, and seawater. The corresponding TOC removal efficiency also slightly decreased from 68.5% in distilled water to 63.7% in Pearl river water, a trend consistent with that of the kinetic rate constant (Fig. 8b). These phenomena might be ascribed to the presence of low concentrations of HCO_3^- or NO_3^- in groundwater, seawater, and Pearl river water that could quench the active free radicals, leading to a decrease in the concentration of ROS for CAP degradation.

The stability and reusability of the electrode is an important indicator of its potential for practical application. Continuous five-cycle operations for CAP degradation were conducted. As can be evinced from Fig. 8c, the removal efficiency of CAP remained stable under continuous operations conditions, and the corresponding TOC removal efficiency also exhibited a similar trend (Fig. 8d). These results suggest that, given its stability and excellent properties, the PbO_2 electrode could be used as a highly effective anode for the removal of CAP contaminants under electro-Fenton-like reaction conditions.

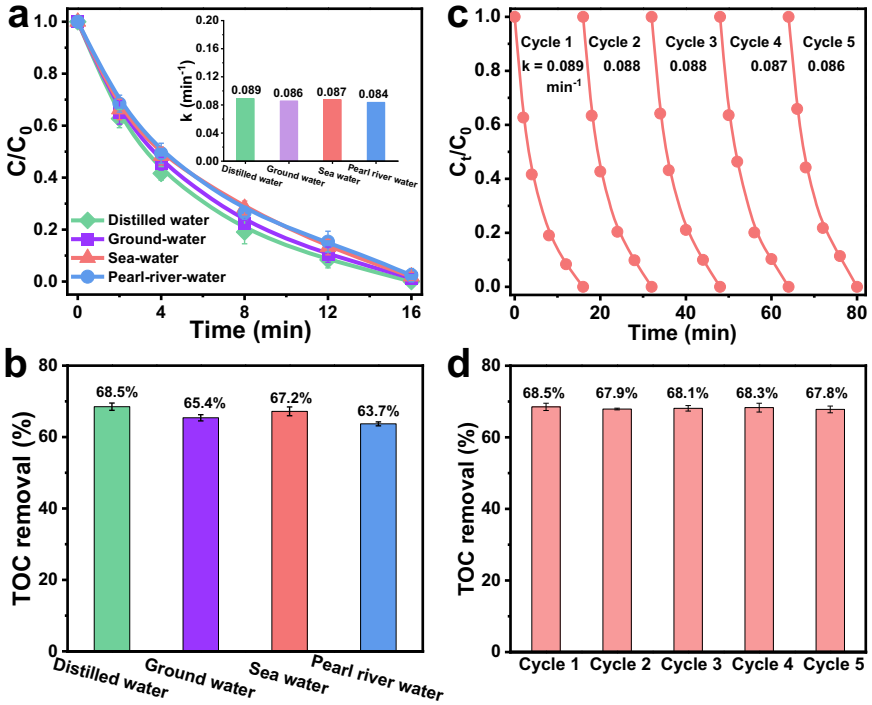

Fig. 8 Exploration of applied potential. a Effect of different water matrices on CAP degradation efficiency and (**b**) the corresponding TOC removal rates. **c** Value of the rate constant of CAP degradation as a function of reaction time over five cycles of continuous operation. **d** The corresponding values for the TOC removal rates. Conditions: initial PMS concentration, 10 mM; initial CAP concentration, 5 mg L^{-1}; current density, 15 mA cm^{-2}; initial Na_2SO_4 concentration, 20 mM L^{-1}; temperature, 27 °C ± 2 °C.

SEM–EDX experiments were conducted to investigate the surface properties of the PbO_2 electrode. As evinced from Supplementary Fig. 6a, before use, PbO_2 had an irregular crystal shape, and this shape did not change obviously after use during the CAP degradation process (Supplementary Fig. 6e). Pb and O were uniformly distributed on the surface of the electrode (Supplementary Fig. 6b–d, f–h), further demonstrating the stability of the PbO_2 electrode during the electro-Fenton-like process. There was no change in the elemental composition of the PbO_2 electrode (as shown in Supplementary Fig. 7) before and after use. This is further supported by the TEM images displaying the irregular crystal shape of the PbO_2 electrode (as shown in Supplementary Fig. 8). We also explored the crystal structure of PbO_2 through XRD (Supplementary Fig. 9a). The major XRD peaks were observed at 2θ = 25.4°, 31.9°, 36.2°, 49.0°, 52.1°, 60.7°, 66.8°, 74.4°, and 78.5°, and they corresponded to the (110), (101), (200), (211), (220), (112), (202), (321), and (222) planes of crystal-type PbO_2 (PDF#41-1492), respectively. After a five-cycle running operation, the peak locations and intensities barely changed, further confirming the stability of the electrode. Additionally, the characteristics of XPS survey spectra suggested that Pb, O, and C elements were distributed on the electrode surface before and after the electro-Fenton-like reaction (Supplementary Fig. 9b). The high-resolution X-ray photoelectron spectra of the Pb (Supplementary Fig. 9c) and O (Supplementary Fig. 9d) elements were characterized by peaks that maintained their intensity and location following the use of the anode in the electro-Fenton-like reaction, suggesting that the PbO_2 electrode was highly stable during the electrochemical reaction that was aimed at antibiotic removal. Evidence indicates that the degradation of CAP in aqueous solutions could be stably and effectively achieved via the electro-Fenton-like reaction using a PbO_2 electrode; notably, to realize the in situ removal of antibiotics from energy-poor regions or from large-area polluted aqueous environments, the removal process can be powered by solar energy.

In summary, an effective electro-Fenton-like reaction process relying on PMS activation and a PbO_2 anode was developed that could be employed for effective and stable CAP degradation. The main findings of this study can be summarized as follows:

i. The electro-Fenton-like process could completely degrade CAP within 16 min with a kinetic rate constant of 0.089 min^{-1} and energy consumption value of 25.1 kWh•m^$^{-3}$.
ii. The CAP degradation performance of the electro-Fenton-like process was highest at 15 mA cm^{-2} current density and 10 mM initial PMS concentration.
iii. When a Na_2SO_4 solution was used as the electrolyte, the kinetic rate constant and TOC removal efficiency were higher than those achieved using $NaHCO_3$ or $NaNO_3$ solutions; this difference was mainly due to the electrode in Na_2SO_4 solution exhibiting excellent electrochemical properties and a high HOMO–LUMO energy gap, resulting in a rapid electron transfer and electrochemical reaction.
iv. The results of quenching experiments and EPR spectroscopy analysis demonstrated that •OH and $SO_4^{\bullet-}$ were the main active species affording CAP degradation; moreover, the contributions to CAP degradation during the electro-Fenton-reaction process of •OH, $SO_4^{\bullet-}$, and electrode-provided electrons were 58.5%, 34.8%, and 6.7%, respectively.
v. Results of quantum chemical calculations indicated that •OH and $SO_4^{\bullet-}$ could be generated through the electrochemical activation of PMS, which could be achieved via electron transfer from CAP to PMS using the PbO_2 electrode.
vi. DFT calculations based on Fukui index analysis and GC–MS information indicated that 6 C, 11 N, and 20 N in CAP were the most likely atoms to be attacked by active species; additionally, evidence suggested that CAP decomposition resulting from the said attacks occurred via two main

pathways, which ultimately led to CAP mineralization to CO_2 and H_2O.

vii. Ecotoxicity evaluations based on developmental factors, fathead minnow LC_{50}, and *T. pyriformis* IGC_{50} analyses suggested that the toxicities of CAP degradation intermediates were significantly lower than that of CAP.

viii. After the continuous operation of the electrochemical system for CAP degradation via the electron-Fenton-like process, the PbO_2 electrode exhibited high stability without obvious leaching of metal ions, which in turn resulted in a stable high kinetic rate constant and TOC removal efficiency.

In summary, not only did this study support the feasibility of continuous run via an electron-Fenton-like process characterized by its stable performance for degrading organic pollutants but also paved the way for the application of the herein-developed process for wastewater treatment and environmental remediation.

METHODS

Materials

HCl, NaOH, HNO_3, $Pb(NO_3)_2$, CAP, 1,4-benzoquinone (BQ), sodium azide (NaN_3), potassium peroxymonosulfate (PMS; $KHSO_5$•0.5KH-SO_4•0.5K_2SO_4, 99%), $NaNO_3$, $NaHCO_3$, Na_2SO_4, methanol (MeOH), *tert*-butanol (TBA), 5,5-dimethyl-1-pyrroline-N-oxide (DMPO), and 2,2,6,6-tetramethyl-4-piperidinyloxyl (TEMP), were purchased from Aldrich-Sigma Reagent Inc.

Preparation of the PbO_2 electrode

A pure Pb plate (Zhengying Technol. Cot. Ltd) was first placed in 20% HCl and then in a 10 g L^{-1} NaOH solution to remove surface oxides and impurities; the Pb plate was then washed with distilled water. Subsequently, it was heated in a muffle furnace at 350 °C for 2 h to cause the formation of an oxide layer on its surface. Electrodeposition was then conducted to prepare the PbO_2 electrode. A three-electrode electrochemical workstation (CS310) was used for this purpose, wherein a Pb plate, Pt wire, and Ag/AgCl electrode were the working, counter, and reference electrodes, respectively. The electrodeposition process was conducted for 1 h at a current density of 20 mA cm^{-2} in a solution containing 0.1 M HNO_3 and 0.5 M $Pb(NO_3)_2$. The obtained electrode was vacuum-dried in an oven for 10 h at 45 °C.

Reactor construction and operation

The electrochemical experiments were conducted in a 350 mL reactor, and 20 mM L^{-1} Na_2SO_4 was used as the electrolyte. The prepared PbO_2 electrode and a stainless-steel mesh were used as the anode and cathode, respectively. The anode–cathode distance was 2.0 cm, and the effective area of the electrodes was 9.0 cm^2. The electrodes were connected by an external circuit equipped with a direct current power source. The impact of various current densities (ranging from 5 to 25 mA cm^{-2}) on the degradation efficiency of CAP was examined. Furthermore, to determine the influence of different electrolytes on CAP degradation, electrolytes such as $NaNO_3$, $NaHCO_3$, and Na_2SO_4 were used with different concentrations (10, 20, 30, and 40 mM L^{-1}) during the EO of CAP. In all experiments, the reactor was operated at room temperature with a stirring apparatus switched on. The samples were extracted and filtered using 0.25 µm millipore filters, and 0.2 mL of MeOH was added into the reaction solution to quench active radicals.

Analytical methods and characterization

CAP concentration was determined through high-performance liquid chromatography (HPLC; Agilent 1200). The HPLC instrument was equipped with an ultraviolet light detector (254 nm) and a C18 column (4.6 × 250 mm; 5 µm). The mobile phase was a water/acetonitrile 70:30 (v/v%) mixture, and the flow rate was 0.5 mL min^{-1}. CAP degradation intermediates were detected via a gas chromatography–mass spectroscopy (GC–MS; Agilent 7890 A GC-5975C). In the relevant experiments, the carrier gas was helium and the flow rate was 1 mL min^{-1}. The injector and ion sources were operated at 185 °C and 200 °C, respectively. The generated ROS were detected via EPR spectroscopy (Bruker, USA) using TEMP or DMPO as the trapping agent. The TOC was determined using a TOC analyzer (TOC-L-CPN, Shimadzu Co, Japan). The leaching metal ion was detected using an inductively coupled plasma–optical emission spectrometer (Thermo Fisher iCAP PRO, USA).

Cyclic voltammetry (CV) experiments were conducted on the anode using an electrochemical workstation and 20 mM L^{-1} Na_2SO_4 solution as the electrolyte. The voltage ranged from −0.5 to 0.5 V, and the scanning rate was 10 mV s^{-1}. Linear sweep voltammetry (LSV) experiments were conducted for 0–2.0 V at a 10 mV s^{-1} scanning rate. Electrochemical impedance spectroscopy (EIS) experiments were performed over a frequency range of 100 kHz–10 Hz at an amplitude of 5 mV. Tafel plots were obtained for −0.3 to 0.3 V at a scanning rate of 1 mV s^{-1}. The surface morphology of the anode before and after use in the CAP degradation process was determined via scanning electron microscopy (SEM) using a microscope (TESCAN MIRA LMS) equipped with an energy-dispersive X-ray spectroscopy (EDX) apparatus. The crystal pattern of the anode was analyzed using an X-ray diffractometer (XRD; Rigaku Ultima IV). The elemental composition and valence state were determined through X-ray photoelectron spectroscopy (XPS; Thermo Scientific K-Alpha).

Quantum chemical simulations

DFT calculations were performed using the Dmol3 program package[44]. The generalized gradient approximation with Perdue–Burke–Ernzerhof formulation was used for the exchange-correlation potentials, and the double numerical polarized (DNP) basis set was operated[45]. A geometry optimization was considered convergent when the force variance was below 0.04 eV $Å^{-1}$. The free energy was calculated using Eq. (6):

$$E_{ads} = E_{total} - E_{substrate} - E_{molecule} \quad (6)$$

where E_{total}, $E_{substrate}$, and $E_{molecule}$ are the total energy of the substrate, the energy of the clean substrate, and the energy of isolated monomer facets, respectively.

The molecular orbital of different reactant was calculated by Gaussian 09 and GaussView at the level of b3lyp with a basis set of 6–31 + g(d, p)[46,47]. The Fukui indices and electrostatic potentials were calculated to predict the reactivity of different sites in CAP[48]. Fukui index values (f_a^-) were calculated based on Eq. (7):

$$f_a^- = q^a_{N-1} - q^a_N \quad (7)$$

where q^a denotes the atom charge of atom a and N represents the charge quantity number[49].

In order to explore the ecotoxicity of CAP and its degradation intermediates, their acute toxicity, lethal concentration, 50% (LC_{50}), developmental toxicity, bioaccumulation factor, and mutagenicity were assessed by quantitative structure–activity relationship (QSAR) predication using the Toxicity Estimation Software Tool (T.E.S.T.) database from the United States Environmental Protection Agency (USEPA)[50].

DATA AVAILABILITY

All data generated or analyzed during this study are available from the corresponding author on reasonable request.

Received: 1 January 2023; Accepted: 2 May 2023;
Published online: 13 May 2023

REFERENCES

1. Yu, J. et al. Efficient degradation of chloramphenicol by zero-valent iron microspheres and new insights in mechanisms. *Appl. Catal. B Environ.* **256**, 117876 (2019).
2. Zhang, J. et al. Ferrate modified carbon felt as excellent heterogeneous electro-Fenton cathode for chloramphenicol degradation. *Water Res.* **227**, 119324 (2022).
3. Xue, Y. et al. Resistance of alkyl chloride on chloramphenicol to oxidative degradation by sulfate radicals: Kinetics and mechanism. *Chem. Eng. J.* **415**, 129041 (2021).
4. Anjali, R. & Shanthakumar, S. Insights on the current status of occurrence and removal of antibiotics in wastewater by advanced oxidation processes. *J. Environ. Manag.* **246**, 51–62 (2019).
5. Zhang, J. et al. Deciphering a novel chloramphenicols resistance mechanism: Oxidative inactivation of the propanediol pharmacophore. *Water Res.* **225**, 119127 (2022).
6. Hofer, U. Chloramphenicol resistance is too hot to handle. *Nat. Rev. Microbiol.* **20**, 381 (2020).
7. Slipko, K. et al. Advanced wastewater treatment with ozonation and granular activated carbon filtration: Inactivation of antibiotic resistance targets in a long-term pilot study. *J. Hazard. Mater.* **438**, 129396 (2022).
8. Geng, R. et al. Adsorption of antibiotics by polydopamine-modified salecan hydrogel: Performance, kinetics and mechanism studies. *Chem. Eng. J.* **454**, 140446 (2023).
9. Tan, Z. et al. Biodegradation mechanism of chloramphenicol by Aeromonas media SZW3 and genome analysis. *Bioresour. Technol.* **344**, 126280 (2022).
10. Dai, C. et al. Construction of a novel integrated electrochemical oxidation-coagulation system for simultaneous removal of suspended solids and antibiotics. *Chem. Eng. J.* **447**, 137505 (2022).
11. Wang, B. et al. Adsorption behaviors of three antibiotics in single and co-existing aqueous solutions using mesoporous carbon. *Environ. Res.* **215**, 114375 (2022).
12. Li, M. et al. Exploring degradation mechanism of tetracycline via high-effective peroxymonosulfate catalysts of montmorillonite hybridized CoFe composites and safety assessment. *Chem. Eng. J.* **427**, 130930 (2022).
13. Wu, Y., Zhou, S., Qin, F., Ye, X. & Zheng, K. Mathematical Model Analysis of Fenton Oxidation of Landfill Leachate. *Waste Manag.* **31**, 468–474 (2011).
14. Li, H. S., Zhou, S. Q., Sun, Y. B. & Lv, J. Nitrogen and carbon removal from Fenton-treated leachate by denitrification and biofiltration. *Bioresour. Technol.* **101**, 7736–7743 (2010).
15. Xu, H. et al. Minimizing toxic chlorinated byproducts during electrochemical oxidation of Ni-EDTA: Importance of active chlorine-triggered Fe(II) transition to Fe(IV). *Water Res.* **219**, 118548 (2022).
16. Lu, J., Hou, R., Wang, Y., Zhou, L. & Yuan, Y. Surfactant-sodium dodecyl sulfate enhanced degradation of polystyrene microplastics with an energy-saving electrochemical advanced oxidation process (EAOP) strategy. *Water Res.* **226**, 119277 (2022).
17. Zhuo, Q., Wang, J., Niu, J., Yang, B. & Yang, Y. Electrochemical oxidation of perfluorooctane sulfonate (PFOS) substitute by modified boron doped diamond (BDD) anodes. *Chem. Eng. J.* **379**, 122280 (2020).
18. Lin, H. et al. Highly Efficient and Mild Electrochemical Mineralization of Long-Chain Perfluorocarboxylic Acids (C9-C10) by Ti/SnO_2-Sb-Ce, Ti/ SnO_2-Sb/Ce-PbO_2, and Ti/BDD Electrodes. *Environ. Sci. Technol.* **47**, 13039–13046 (2013).
19. Liu, L. et al. The efficient degradation of sulfisoxazole by singlet oxygen ($^1O_2$) derived from activated peroxymonosulfate (PMS) with Co_3O_4-SnO_2/RSBC. *Environ. Res.* **187**, 109665 (2020).
20. Shin, Y. U. et al. Electrochemical oxidation of organics in sulfate solutions on boron-doped diamond electrode: Multiple pathways for sulfate radical generation. *Appl. Catal. B Environ.* **254**, 156–165 (2019).
21. Fu, X., Han, Y., Xu, H., Su, Z. & Liu, L. Electrochemical study of a novel high-efficiency PbO_2 anode based on a cerium-graphene oxide co-doping strategy: electrodeposition mechanism, parameter optimization, and degradation pathways. *J. Hazard. Mater.* **422**, 126890 (2022).
22. Rahmani, A. et al. Improved degradation of diuron herbicide and pesticide wastewater treatment in a three-dimensional electrochemical reactor equipped with PbO_2 anodes and granular activated carbon particle electrodes. *J. Clean. Prod.* **322**, 129094 (2021).
23. Wan, C., Zhao, L., Wu, C., Lin, L. & Liu, X. Bi5+ doping improves the electrochemical properties of Ti/SnO_2–Sb/PbO_2 electrode and its electrocatalytic performance for phenol. *J. Clean. Prod.* **380**, 135005 (2022).
24. Rong, H. et al. Electrochemical degradation of Ni-EDTA complexes in electroless plating wastewater using PbO_2-Bi electrodes. *Chem. Eng. J.* **431**, 133230 (2022).
25. Hua, G. et al. Fabrication and characterization of porous titanium-based PbO_2 electrode through the pulse electrodeposition method: Deposition condition optimization by orthogonal experiment. *Chemosphere* **261**, 128157 (2020).
26. Zhong, D. et al. Study on degradation of chloramphenicol by H_2O_2/PMS double-oxidation system catalyzed by pipe deposits from water networks. *J. Environ. Chem. Eng.* **10**, 107529 (2022).
27. Hu, X. et al. N- and O self-doped biomass porous carbon cathode in an electro-Fenton system for Chloramphenicol degradation. *Separ. Purif. Technol.* **251**, 117376 (2020).
28. Wang, C., Yin, L., Xu, Z., Niu, J. & Hou, L. A. Electrochemical degradation of enrofloxacin by lead dioxide anode: Kinetics, mechanism and toxicity evaluation. *Chem. Eng. J.* **326**, 911–920 (2017).
29. Wang, K., Huang, D., Wang, W., Ji, Y. & Niu, J. Enhanced perfluorooctanoic acid degradation by electrochemical activation of peroxymonosulfate in aqueous solution. *Environ. Int.* **137**, 105562 (2020).
30. Li, M., Zhou, J., Bi, Y.-G., Zhou, S.-Q. & Mo, C.-H. Polypyrrole/sewage sludge carbon as low-cost and high-effective catalyst for enhancing hexavalent chromium reduction and bio-power generation in dual chamber microbial fuel cells. *Separ. Purif. Technol.* **256**, 117805 (2021).
31. Zhuang, Y., Wang, X., Zhang, L., Kou, Z. & Shi, B. Confinement Fenton-like degradation of perfluorooctanoic acid by a three dimensional metal-free catalyst derived from waste. *Appl. Catal. B Environ.* **275**, 119101 (2020).
32. Duan, P. et al. Enhanced degradation of clothianidin in peroxymonosulfate/catalyst system via core-shell FeMn @ N-C and phosphate surrounding. *Appl. Catal. B Environ.* **267**, 118717 (2020).
33. Qin, C. et al. DNA Facilitates the Sorption of Polycyclic Aromatic Hydrocarbons on Montmorillonites. *Environ. Sci. Technol.* **52**, 2694–2703 (2018).
34. Ayyappan, S., Sundaraganesan, N., Aroulmoji, V., Murano, E. & Sebastian, S. Molecular structure, vibrational spectra and DFT molecular orbital calculations (TD-DFT and NMR) of the antiproliferative drug Methotrexate. *Spectrochim. Acta* **11**, 264–275 (2010).
35. Yang, Z., Qian, J., Yu, A. & Pan, B. Singlet oxygen mediated iron-based Fenton-like catalysis under nanoconfinement. *Proc. Natl Acad. Sci. USA* **116**, 6659–6664 (2019).
36. Li, M. et al. Efficient decomposition of perfluorooctane sulfonate by electrochemical activation of peroxymonosulfate in aqueous solution: Efficacy, reaction mechanism, active sites, and application potential. *Water Res.* **221**, 118778 (2022).
37. Asif, M. B., Kang, H. & Zhang, Z. Gravity-driven layered double hydroxide nanosheet membrane activated peroxymonosulfate system for micropollutant degradation. *J. Hazard. Mater.* **425**, 127988 (2022).
38. Wang, Y. et al. A novel peroxymonosulfate (PMS)-enhanced iron coagulation process for simultaneous removal of trace organic pollutants in water. *Water Res.* **185**, 116136 (2020).
39. Wen, Y. et al. Piezo-enhanced photocatalytic performance of ZnO nanorod array for pollutants degradation in dynamic water: Insight into the effect of velocity and inner flow field. *Nano Energy* **101**, 107614 (2022).
40. Li, S., Huang, T., Du, P., Liu, W. & Hu, J. Photocatalytic transformation fate and toxicity of ciprofloxacin related to dissociation species: Experimental and theoretical evidences. *Water Res.* **185**, 116286 (2020).
41. Duan, X., Sun, H. & Wang, S. Metal-Free Carbocatalysis in Advanced Oxidation Reactions. *Acc. Chem. Res.* **51**, 678–687 (2018).
42. Zheng, Z. et al. Guanidinocalix[5]arene for sensitive fluorescence detection and magnetic removal of perfluorinated pollutants. *Nat. Commun.* **10**, 5762 (2019).
43. Cai, Z. et al. Highly active WO_3@anatase-SiO_2 aerogel for solar-light-driven phenanthrene degradation: Mechanism insight and toxicity assessment. *Water Res.* **162**, 369–382 (2019).
44. Aihara, J. Reduced HOMO-LUMO gap as an index of kinetic stability for polycyclic aromatic hydrocarbons. *J. Phys. Chem. A* **103**, 7487–7495 (1999).
45. Ricca, C. et al. B, N-Codoped graphene as catalyst for the oxygen reduction reaction: Insights from periodic and cluster DFT calculations. *J. Comput. Chem.* **39**, 637–647 (2018).
46. Frisch, M. et al. Gaussian 09, Revision D. 01. Gaussian. Inc., Wallingford CT. 201. (2009)
47. Li, M. et al. Exploration of perfluorooctane sulfonate degradation properties and mechanism via electron-transfer dominated radical process. *Water Res.* **215**, 118259 (2022).
48. Gonzalez, C. & Schlegel, H. B. An improved algorithm for reaction path following. *J. Chem. Phys.* **90**, 2154–2161 (1989).
49. Lu, T. & Chen, F. M. Multiwfn: A Multifunctional Wavefunction Analyzer. *J. Comput. Chem.* **33**, 580–592 (2012).
50. Ma, J. et al. Oxygen defective titanate nanotubes induced by iron deposition for enhanced peroxymonosulfate activation and acetaminophen degradation:

Mechanisms, water chemistry effects, and theoretical calculation. *J. Hazard. Mater.* **418**, 126180 (2021).

ACKNOWLEDGEMENTS

We gratefully thank the financial support from Project Funded by Key Program of National Natural Science Foundation of China (42030713), National Natural Science Foundation of China (42007358), Guangdong Basic and Applied Basic Research Foundation (2020A1515110518), the Hong Kong Scholarship Program (XJ2020059), and the China Postdoctoral Science Foundation (2019M663382). KLY acknowledges the Project of Hetao Shenzhen-Hong Kong Science and Technology Innovation Cooperation Zone (HZQB-KCZYB-2020083). SQZ thanks the project of the State Key Research & Development Project of China (2022YFC3705003) and the Project funded by the Department of Science & Technology of Guizhou Province (2023-115). The authors would like to thank Shiyanjia Lab (www.shiyanjia.com) for XPS measurements.

AUTHOR CONTRIBUTIONS

M.L., J.C., and J.S. designed and conducted all the preparation, characterization, and measurements. M.L. and C.M. wrote and revised the whole manuscript. N.F., S.Z., and H.Z. brought a clear study pathway and guided the project. Z.Z., W.H., and Q.W. help analyse the data. K.Y., S.Z., and C.M. guided the project.

COMPETING INTERESTS

The authors declare no competing interests.

ADDITIONAL INFORMATION

Supplementary information The online version contains supplementary material available at https://doi.org/10.1038/s41545-023-00255-9.

Correspondence and requests for materials should be addressed to Meng Li, King Lun Yeung, Shaoqi Zhou or Ce-Hui Mo.